Biosensors and Bioelectronics 133 (2019) 215–222

Contents lists available at ScienceDirect

Biosensors and Bioelectronics

journal homepage: www.elsevier.com/locate/bios

Ultra-sensitive electrochemical detection of bacteremia enabled by redox-active gold nanoparticles (raGNPs) in a nano-sieving microfluidic system (NS-MFS)

Chun-Wei Lee[a,b], Hwan-You Chang[c], Jen-Kuei Wu[a,b,*], Fan-Gang Tseng[a,b,d,*]

[a] Department of Engineering and System Science, National Tsing Hua University, Hsinchu, Taiwan ROC
[b] Frontier Research Center on Fundamental and Applied Sciences of Matters, National Tsing Hua University, Hsinchu, Taiwan ROC
[c] Department of Medical Science, National Tsing Hua University, Hsinchu, Taiwan ROC
[d] Division of Mechanics, Research Center for Applied Sciences, Academia Sinica, 128 Academia Road, Section 2, Nankang, Taipei 115, Taiwan, ROC

ARTICLE INFO

Keywords:
Amperometric biosensor
Electropolymerized self-assembled layer
Bacteremia
Nano-sieving microfluidic system
Redox-active gold nanoparticles

ABSTRACT

Early diagnosis of bacterial infections is crucial to improving survival rates by enabling treatment with appropriate antibiotics within the first few hours of infection. This paper presents a highly sensitive amperometric biosensor for the detection of several pathogenic bacterial cells in blood plasma around 30 min. The proposed device is based on an electropolymerized self-assembled layer on gold nanoparticles operated in a portable nano-sieving microfluidic system (NS-MFS). The redox-active gold nanoparticles (raGNPs) enhanced the electrical conductivity and provided a greater number of electrochemically active molecules for sensing, while improving resistance to the fouling of sensors by oxidation products in blood plasma. The detection limit of the device has been shown to reach 10 CFU/mL for *Pseudomonas aeruginosa* and *Staphylococcus aureus* spiked in plasma. The dynamic range of the sensing system falls between 10 and 10^5 CFU/mL in a buffer solution by cyclic voltammetry (CV) measurements. The results demonstrated that the raGNPs/NS-MFS can successful detect *P. aeruginosa* and *S. aureus* in human plasma, and is very useful for the diagnosis of bacteremia from clinical samples.

1. Introduction

Bacterial infection remains a major threat to human health, despite recent advances in medical diagnostics and therapeutic technologies. Bacterial invasion into human circulatory system (referred to as bacteremia), often has serious consequences, including death. Bacteremia diagnosis commonly relies on bacteria cultures and, biochemical characterization that can take several days to complete (Murray and Masur, 2012). Thus, developing a rapid, sensitive, and simple method based on microfluidics for the detection of bacterial pathogens in whole blood will be highly valuable (Hou et al., 2011; Phaneuf et al., 2016). Nonetheless, the direct detection of small numbers of live bacteria in clinical blood or urine samples remains a serious challenge (Lazcka et al., 2007). Two major difficulties in the rapid detection of trace quantities of bacteria are (i) short- to real-time detection and (ii) the need for ultrasensitive bioanalysis (Afshari et al., 2012; Sin et al., 2014). Simplifying the sample preparation process is crucial to reducing the time required for target detection. However, the sensitivity of detection must be sufficiently high to eliminate the need for target amplification and enrichment. Several techniques have recently been developed to amplify analytical signals from biorecognition events in order to improve the sensitivity of bioassays used in the detection of bacteria (Lim et al., 2015; Wang et al., 2013; Zhao et al., 2004). One common method to detect small numbers of bacteria is to use nanoparticles (NPs) to enhance the signals obtained from captured bacteria. NPs with specific optical (Sanvicens et al., 2009), electrochemical (Zhao et al., 2004) or magnetic (Sage et al., 2014) properties can increase the speed and sensitivity of detection in diagnostic methods. Moreover, the ability to combine NPs facilitates their implementation into point-of-care systems and multiplexed devices. For example, NPs labelled with monoclonal antibodies are commonly used in immunochromatographic strip to detect pathogenic bacteria in which the color intensity is positively proportional to the concentration of analyte that can be judged by naked eyes or a strip reader (Wang et al., 2015, 2016a, 2016b, 2017).

A variety of electrochemical biosensing schemes using enzymes and colloidal metal NPs as labels have been reported (Maalouf et al., 2007; Lee et al., 2009; Saha et al., 2012; Xu et al., 2016). Metal NPs are widely

* Corresponding authors at: Department of Engineering and System Science, National Tsing Hua University, Hsinchu, Taiwan ROC.
E-mail addresses: jkwu@mx.nthu.edu.tw (J.-K. Wu), fangang@ess.nthu.edu.tw (F.-G. Tseng).

https://doi.org/10.1016/j.bios.2019.03.040
Received 2 January 2019; Received in revised form 18 March 2019; Accepted 19 March 2019
Available online 20 March 2019
0956-5663/

employed for their excellent conductivity, which enables them to act as "electronic wires" capable of promoting communication between the redox centers in proteins and electrode surfaces. The catalytic activity of metal NPs also enables the amplification of electrochemical reactions. In one study, a system based on screen-printed carbon electrodes modified with gold nanoparticles (GNPs) resulted in a 13.1-fold increase in the detection of *Escherichia coli* O157:H7 than without gold NPs and exhibited a working range of 10^2–10^7 CFU/mL (Xu et al., 2016). The bacteria were detected by platinum-coated gold nanoporous electrodes with a limit of detection (LOD) of 10 CFU/mL (Maalouf et al., 2007). In another system, a rigid, conductive gold nanocomposite was shown to have excellent transducing properties, as demonstrated by the detection of Salmonella at pM levels (Saha et al., 2012). These methods take the advantage of large surface area from NPs to improve LOD; moreover, a greater gain in terms of speed, selectivity, and detectability can be obtained but sophisticated/expensive instruments are required. The other issue is the need to maintain a low signal to noise ratio when blood and urine samples are applied directly to sensors. Conventional fluorescence-based immunoassays such as enzyme-linked immunosorbent assay (ELISA) require large sample volumes and diluent to prevent interference from cross-contamination of other components (Vainshtein and Lee, 2014; Vasudev, 2013). Electrochemical immunoassays usually require a smaller amount of samples; however, they suffer from strong background noise (Das et al., 2006) because of the amplified signals involving enzymes for mediating communication (Zhuang et al., 2015) or catalysts to improve redox reactions (Goggins et al., 2015). As a result, the sensitivity is roughly 10^3 to 10^6 CFU/mL (Das et al., 2006) by using special enzymes or 10^2 to 10^7 CFU/mL by using engineered catalysts (Zhuang et al., 2015), which barely reaches the clinical detection requirements of 1–100 CFU/mL. Enabling the detection of single bacterium requires not only enhancing effective signals from electrochemical reactions, but also reducing the background noise caused by oxidation products from medium or plasma.

This study proposes a strategy based on signal amplification by conjugating an electrochemical active molecule (EAM) and a specific antibody on redox active gold nanoparticles (raGNPs). The modified raGNPs are conjugated to the surface of bacteria via a specific antibody to form an electrochemically active poly-film by electropolymerization. When applying a voltage, a redox-active current of the EAM film can be detected by a conventional electrochemical detection system typically in a range between nA and mA.

A functional EAM, either redox active self-assembled monolayer (SAM) such as 5-amino-2-mercapto-1,3,4-thiadiazole or 4-aminothiophenol molecule, is arranged on GNP surfaces. Each GNP contains thousands of EAMs; therefore, the signal from individual bacterium can be enhanced by six orders of magnitude at an optimized condition (ligand binding sites on each bacteria surface could be more than hundreds for GNPs to conjugate). Likewise, the self-assembled EAMs cover nearly the entire surface of the electrodes, thereby preventing direct contact with solutions, such that antifouling of the modified electrodes can be anticipated. As a result, background noise associated with interference from oxidation products in the medium or plasma can be reduced (Goggins et al., 2015).

A schematic diagram of the proposed biosensing principle is presented in Fig. 1. This approach enables the detection of small numbers of bacteria thanks to the large number of electrochemically active molecules ($10^{5–6}$ molecules/cell) associated with each bacterium, such that the oxidation current signal can be measured within a normal range of sensitivity (μ A-nA), without the need for highly sensitive signal detection equipment (< pA) to measure analytes at very low concentrations (pM-fM). The proposed raGNPs also does not require electrochemical transfer media or special catalysts for signal enhancement.

This study used a filtration device comprising an array of carbon nanotubes as a filter for bacteria purification, in which only non-conjugated gold nanoparticles (30 nm) could pass through a filter with 100–200 nm pores thus leave the conjugated GNP/bacteria complex to retain in an incubation chamber for detection. These functions were integrated inside a microfluidic system for rapid detection of bacteria.

2. Experimental

2.1. Chemicals and cell culture

All reagents used in this study were of analytical grade and the solutions were prepared using deionized water. Prior to each experiment, all solutions were filtered using 0.22 μm syringe filters (Whatman, NJ, USA). Two redox-active self-assembled monomers, 5-amino-2-mercapto-1,3,4-thiadiazole (AMT) and 4-aminothiophenol (4-ATP) were purchased from Sigma-Aldrich (MO, USA). Gold nanoparticles (30 nm in diameter stabilized in a suspension of citrate buffer) were obtained from Sigma-Aldrich (MO, USA). 10 mM 4-(2-Hydroxyethyl)-piperazine-1-ethanesulphonic acid (HEPES, Sigma, MO, USA) was prepared as a running buffer and adjusted to pH 7.5 using 0.1 M NaOH. *Pseudomonas aeruginosa* PAO1 (PA) and *Staphylococcus aureus* (SA, SA-BCRC No. 16014) were laboratory stock and were routinely grown in Luria-Bertani medium (BD Difco™, Cat. No 244610) at 37 °C for 16–18 h under shaking at 150 rpm. Mouse anti-Pseudomonas aeruginosa antibody (Clone B11, Catalog # MA1-83430) was purchased from ThermoFisher Scientific. FITC-conjugated goat anti-mouse IgG antibody, and mouse anti-Staphylococcus aureus antibody (Clone 704, Catalog # ab37644) were purchased from Abcam.

2.2. Chip design and fabrication

The channel of the HSBD chip comprised a polydimethylsiloxane (PDMS) cover bound with SiO_2 nano-channels fabricated on a silicon substrate, as shown in Fig. 2(a)(b). This chip includes an incubation chamber connected to a loading channel via a filter valve comprising an array of multi-walled carbon nanotubes (MWCNTs). The chips were fabricated on a silicon wafer using standard photolithographic and microfabrication processes in conjunction with the in-situ growth of MWCNTs nanostructures as a sieving filter for GNPs, as shown in Fig. S2. The construction of microchannels (2.5-cm long and 100-μm wide) was performed by patterning the channel with a 10-μm thick film of AZ9260 resist (Microchem Corp., USA) as an etching mask, followed by reactive ion etching (RIE) (SF_6: 10 sccm and O_2: 2 sccm for 600 s) to produce a channel 5–10 μm in depth. Prior to the deposition of catalyst metals for the growth of CNTs, the silicon channel was covered with a thin layer of SiO_2 (about 500 nm) by Plasma-Enhanced Chemical Vapor Deposition (PECVD) process. Layers of Ti, Al, and Ni metal catalysts (thicknesses of 1500, 200, and 100 Å, respectively) were consecutively deposited by e-gun evaporation on the surface patterned by photoresist for the growth of MWCNTs with layers for adhesion, electron conduction, and catalysis. Following the removal of the photoresist by a lift-off process, the catalyst layer remained only at the bottom of the channel in selected regions. The in-situ growth of MWCNTs was performed by chemical vapor deposition (CVD), as previously described (Gzil et al., 2003; Zhang et al., 2003). Chips were patterned on a standard silicon wafer with a 0.5 μm top layer of PECVD $Si0_2$. The silicon dioxide provides insulation between the electrodes and facilitates a stronger bond with the PDMS. Working electrodes were patterned by first using DC sputtering to deposit 50 nm of chromium, followed by 300 nm of Indium Tin Oxide (ITO) across the wafer then etched to retain the selected regions. Reference and counter electrodes were patterned by image-reversal photoresist AZ5214 and lift-off process was used to define the locations with 50 nm thick chromium and 100 nm thick platinum. Finally, the PDMS cover slip was treated with O_2 plasma (O_2: 30 s, 10 sccm flux; P1000E RIE system, Branchy, Taiwan) to provide a reversible, hydrophilic bonding between the PDMS and the silicon substrate in order to ease the peeling process and avoid leakage. Prior to bonding, four holes were drilled at the end of the channels for use as

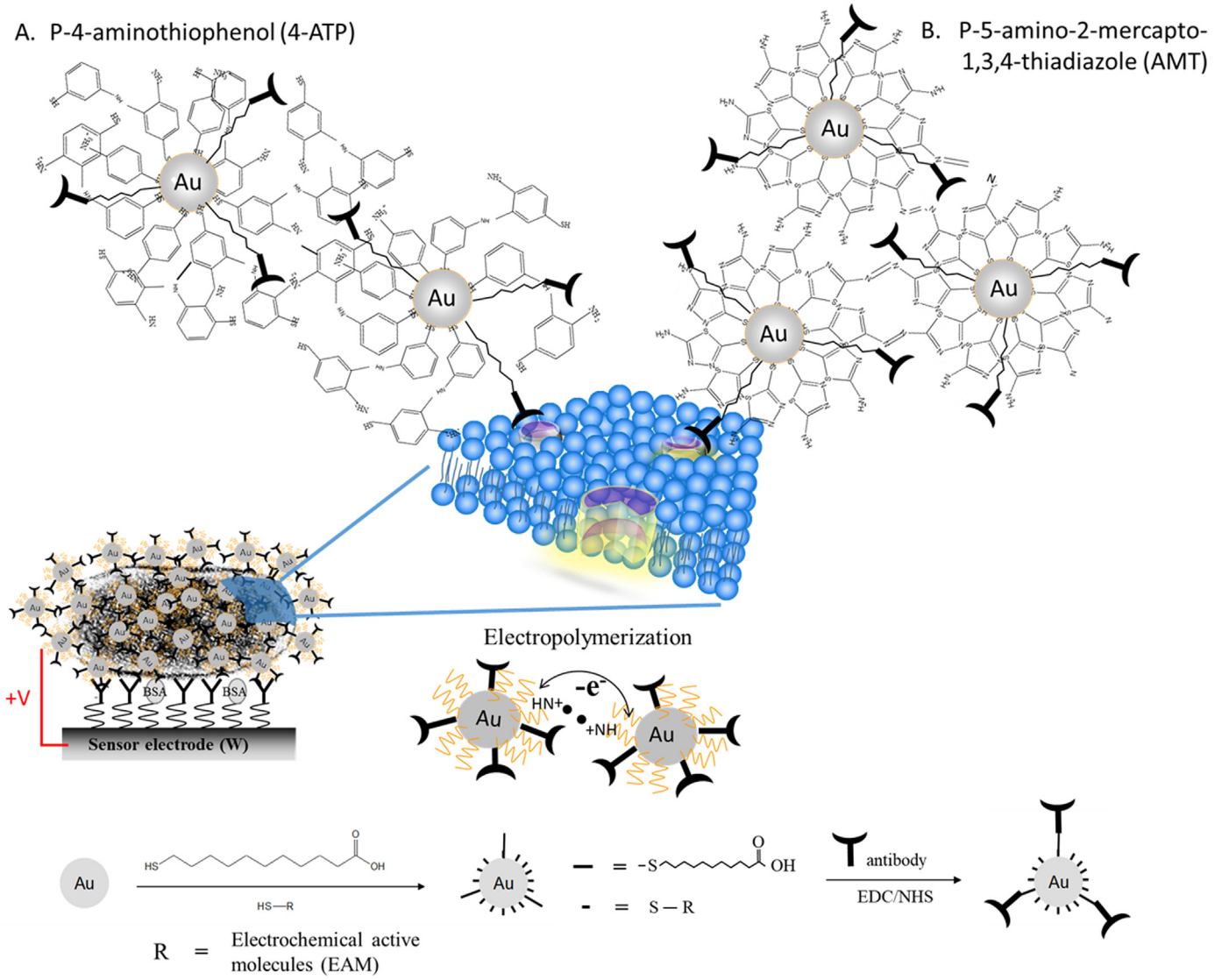

Fig. 1. Structure and mechanism of (A) 4-aminothiophenol (4-ATP), or (B) 5-amino-2-mercapto-1,3,4-thiadiazole (AMT) monolayer electropolymerized on GNPs as an electrochemical sensor for highly sensitive bacteria detection (HSBD).

sample reservoirs. The key features of the proposed system are presented in Fig. 2.

2.3. Analytical procedure

A spiked sample of blood plasma with P. aeruginosa (PAO1) and S. aureus (SA-BCRC No. 16014) was diluted in HEPES buffer at a ratio of 1:10. The dilution was calibrated for all stepwise concentration experiments. The redox active-SAM monomer, AMT and 4-ATP conjugated with gold nanoparticles (GNPs) are conducted through the covalent bonds formed between thiol group and gold; subsequently the specific antibodies (Mouse monoclonal to P.aeruginosa, Mouse monoclonal to S. aureus) were used to conjugate to gold nanoparticles via the activation of 11-mercaptoundecanoic acid (2 mM) with EDC (1-Ethyl-3-(3-dimethylaminopropyl)-carbodiimide) and sulfo-NHS (N-hydroxysulfosuccinimide), Sulfo-NHS enhances the effectiveness of EDC and binds to EDC after it binds a carboxyl group and a free amino group. Then EDC/sulfo-NHS chemistry was used to immobilize antibodies (Vashist, 2012). The Binding efficiency of GNPs-Antibody-FITC attached onto the surface of bacteria is shown in Fig. S3, with a concentration of 800 nM sufficient for saturating the bacterial surface. The HSBD chip underwent consecutive filtering (typically 20 μL) and washing (normally 1 mL) with phosphate-buffered saline (PBS) buffer for GNPs-Bacteria conjugates to retain in front of a CNT filter (gap size of 100–200 nm) and remove non-conjugated raGNPs. Further elution of the retained bacteria was accomplished by passing 5–10 mL of PBS in the direction opposite to that of the initial filtering, and injecting the outgoing solution of eluted bacteria in PBS directly into the measurement chamber for electrochemical detection by a bipotential electrochemical workstation (CHI 760B). The detailed operation process flow of the HSBD microfluidic chip is shown in Fig. S4.

3. Results and discussion

3.1. Bacteria enrichment and purification

To enhance detection sensitivity and streamline analysis procedures, this study developed a chip-based filtration system using an array of MWCNT nanopillars at the edge of the incubation chamber. The MWCNT filter has two functions. First, it is used to concentrate bacteria in the incubation chamber to facilitate antibody recognition and the detection of a small number of bacteria from high-volume samples. Second, the filter enables the on-chip separation of bacteria from unconjugated gold nanoparticles, thereby eliminating the need for

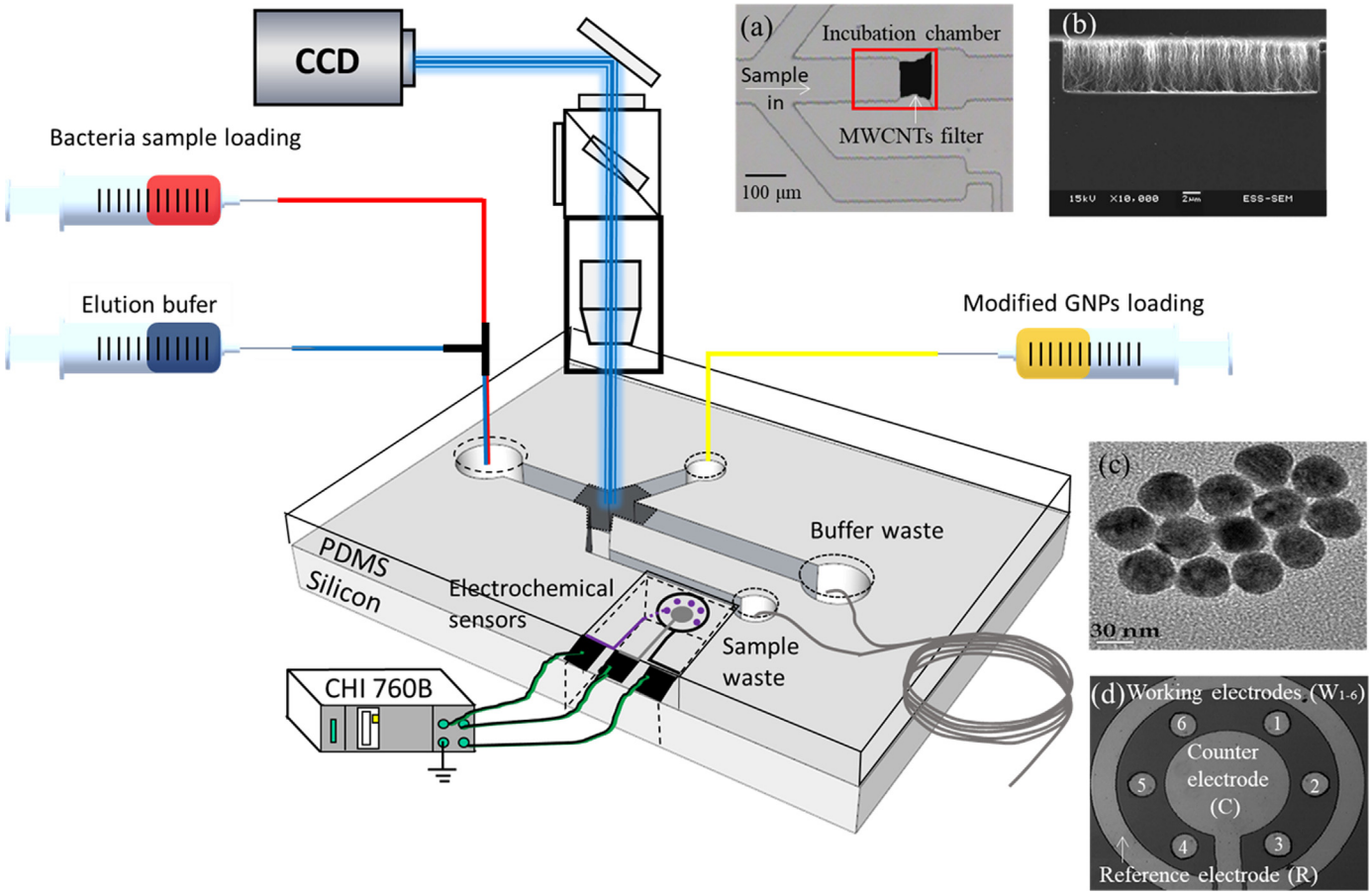

Fig. 2. Images and operation of NS-MFS chip: (a) Top view optical microscope image of the incubation chamber with MWCNT nano-pillar filter; (b) Cross-section SEM image of CNTs-filter grown in microchannel; (c) SEM of raGNPs; (d) Top view of the arrayed electrodes; (e) Schematic diagram of HSBD, showing the incubation and filtration processes of raGNPs conjugated on bacteria. Flow processing: (1) simultaneous loading modified raGNPs and samples; (2) filtration of samples and removal of non-conjugated raGNPs; (3) incubation and transfer of samples to detection channel.

off-chip purification procedures. Bacteria and bacteria-conjugated raGNPs are held by the filter (gap size of 100–200 nm), while excess raGNPs (30 nm) could pass through. Following the repeated injection of buffer solutions to wash off unbound raGNPs, the MWCNT filter is backwashed to remove the captured bacteria for detection. Fig. 3 presents an example of sample purification and enrichment using a MWCNT Filter. Following sample loading (bacteria and antibody-conjugated raGNPs), the microfluidic channel was flushed with PBS to remove unbound raGNPs. The target bacteria conjugated with raGNPs by the first-antibody confined in the incubation chamber in front of the MWCNT filter, whereupon the direction of flow through the elution buffer was reversed to wash out captured bacteria for electrochemical measurement. A fluor-dye labelled secondary antibody in elution buffer was used to identify *P. aeruginosa* and *S. aureus* following incubation. The fluor-images of bacteria/raGNPs conjugates were obtained only when the fluor-dye labelled secondary antibodies were bound to the first-antibody. As shown in Fig. 3(a)(b), bacteria concentrated before MWCNT filter and only GNPs percolate through to downstream.

The spiked sample was sequentially passed through the collection channel, and the amperometric signal was amplified by EAMs conjugated on the surface of bacteria that were captured by the antibody-conjugated electrodes, as shown in Fig. 3(c)(d).

Control tests were also performed to verify whether the cyclic voltammetry signal was obtained exclusively from the bacterial (*S. aureus* (SA) and *P. aeruginosa* (PA) under 1000 CFU/mL) recognition event (blue and red, 1 + 2 + 3) of the biosensor rather than from the non-specific absorption of target bacteria (black line, 1 + 3) or the leakage of residual raGNPs-Ab (green and purple line, 2 + 3) during the filtration step. The redox performance of bacteria in five different conditions by cyclic voltammetry is presented in Fig. 4. Background noise caused by unbounded raGNPs was determined according to the measurement of leakage current and cyclic voltammetry. It appears that the redox currents of particle-conjugated bacteria are nearly unaffected by background current. On the other hand, the redox current decreases gradually with the increment of cycle numbers and eventually come to a saturation condition at the end of tenth cycle, indicating the chip can not only effectively increase purification capacity but also limit leakage effect.

3.2. Characteristics of electroactive molecules on raGNPs

The covalent attachment of 5-amino-2-mercapto-1,3,4-thiadiazole (AMT), and 4-aminothiophenol (4-ATP) on GNPs was performed via a thiol-metal self-assembly procedure (Vashist, 2012). The electrochemical properties of this monolayer were investigated using cyclic voltammetry (CV). Fig. 5(a) presents a typical cyclic voltammogram (CV) of AMT GNPs (100 nM AMT + 0.05 M H_2SO_4 + 0.1 M HEPES buffer with 10^3 to 10^{-4} particles/μL) electropolymerization on the surface of ITO electrodes. The two cation radicals on the AMT were coupled to form a dimer via a hydrazone-bond after a voltage was applied. The oxidation of the two NH_2 groups on the AMT leads to the formation of dimer species on the surface of the electrode (Li et al., 2017). The oxidation of SH group occurs in the window between 0.2 and 0.6 V; therefore, it could be expected that the observed redox peak is due to a redox reaction of thiol group to form disulfide bond. We observed three oxidation peaks at 0.2, 0.5 and 0.8 V in the forward scan

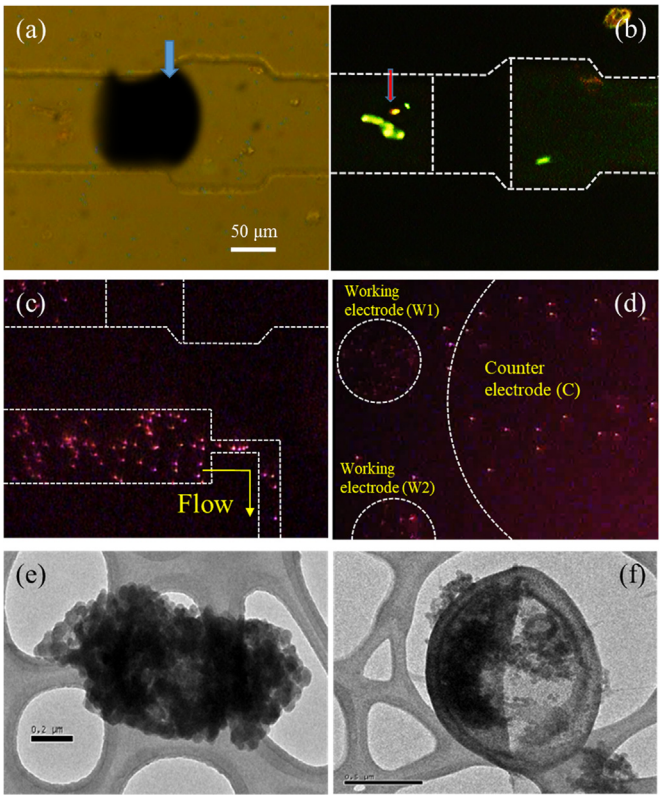

Fig. 3. Bright field (a) and fluorescence (b) microscopic images of fluor-dye labelled *P. aeruginosa* (marked by a red arrow in b) concentrated in front of the MWCNT nanopillar array (gap size of 100–200 nm, the dark area marked with a blue arrow). The scale bar is 50 μm. The bacteria attached to raGNPs were sequentially passed through the collection channel (c), and the target bacteria were captured by antibody-conjugated electrodes. The direction of fluid flow in the channel is indicated by an arrow. Dotted lines are used to outline the relative locations of channels and electrodes. TEM images of nanoparticles binding on (e) *P. aeruginosa* and (f) *S. aureus*.

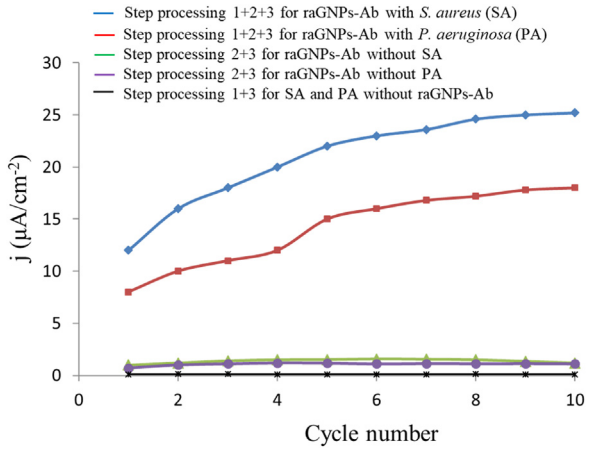

Fig. 4. Plot of specific redox capacitance vs. cycle numbers for different combinations of operation processes. The scanning rate is 50 mV s-1 at ± 1 V. Only complete process (1 + 2 + 3) can provide significant current-density signals rather than (2 + 3) or (1 + 3). (flow processes: 1. loading modified raGNPs and samples, 2. filtration of samples and removal of non-conjugated raGNPs, 3. incubation and transfer of samples into detection channel).

and one reduction peak at −0.1 V in the reverse scan. At larger positive electrode potentials (over 1.0 V), an anodic wave was observed, which is presumably due to the desorption of polymerized AMT (p-AMT)-GNPs from the surface and concomitant oxidation reaction. One previous study identified the oxidation of a p-AMT-GNPs modified glassy carbon (GC) electrode at 300–800 mV (Revin andJohn, 2011).

A CV was recorded during the electropolymerization in the presence of 4-aminothiophenol (100 nM 4-ATP + 0.05 M H_2SO_4 + 0.1 M HEPES buffer with 10^3 to 10^{-4} particles/μL) at a scanning rate of 100 mV/s, as shown in Fig. 5(b). The anodic peak observed in the first cycle could be assigned to the electrochemical oxidation of the hydrolytic cleavage of the imine moiety to give the corresponding surface-bound quinone monoimine (Lukkari et al., 1998). An electrochemical polymerization process was used to form a polymerized ATP (P-ATP) GNPs film on ITO electrodes. A film of P-ATP GNPs was deposited by repetitively sweeping the potential from − 0.2 to 1.0 V at a scanning rate of 100 mV s^{-1}. An irreversible oxidation process appeared during the first cycle and disappeared during the second cycle. The reduction peak at 0.33 V may have been caused by the catalyzing of p-ATP polymerization by GNPs. An oxidation peak of p-ATP was clearly observed at potentials of 0.38 V and 0.58 V in the first scan. These results demonstrate the formation and bonding of a compact polymeric film to the surface of the electrode. The decrease in peak current appears to be related to the continual formation of P-ATP GNPs composite membranes leading to the suppression of the voltammetry response. The current gradually decreased with the number of scan cycles, eventually reaching a steady state.

3.3. Selectivity and sensitivity analysis of HSBD biosensor

Selectivity was evaluated by exposing the antibody-immobilized multi-array electrodes to *P. aeruginosa* (PA) and *S. aureus* (SA) under the following conditions: (I) a mixture solution of raGNPs-Ab (antibody conjugated GNPs (10^{3-4} particles/μL) in 100 nM electropolymerized redox-active SAM solution, total volume 100 μL) and bacteria sample (SA or PA), (II) pure bacteria sample solution without raGNPs-Ab, and (III) only raGNPs-Ab standard solution. CV illustrates the relationship between the electropolymerizated EAM layer and signal enhancement under three different conditions, in which the sample concentration was 10 CFU/mL diluted in HEPES buffer.

To evaluate the issue of non-specific interaction, plain electrodes were exposed to target bacteria with stepwise increases in concentration. Serum testing for the identification of bacteria was conducted using actual samples (Fig. 6(A) & B; (a) raGNPs-Ab with bacteria matching target (with a dynamic range 10–10^5 CFU/mL), (b) raGNPs-Ab with target mismatch, (c) raGNPs-target bacteria; and (d) pure target bacteria) from 0 up to 10^5 CFU/mL); however, no response was observed. These results demonstrate that no cross-reactivity occurred when detecting these two pathogenic bacteria, indicating the high selectivity of the biosensor for this specific antibody (PA, Fig. 6(A); SA, Fig. 6B).

3.4. Detection limits of HSBD biosensor

Samples of bacteria (PA and SA, with a concentration of 1.3 × 10^6 CFU/mL in 20 mM HEPES buffer solution) were diluted to 10–100 CFU/mL using blood plasma and PBS, as shown in Fig. 7. Peaks were measured in the electrochemical current at 0.8–1.0 V for p-AMT and 0.6–0.8 V for p-ATP resulting from cation-radical interactions (Inzelt, 2008). The amperometric responses in blood plasma is lower than in HEPES buffer probably due to non-specific binding of plasma proteins on the surface of working electrode to lower down the efficiency for electrochemical detection of bacteria. Yet this situation carries out only minor effects on the signals, and the sensors can still respond to different level of bacteria robustly, according to the calibration results shown in Fig. 6. From analysed SEM images in Fig. 3(e)(f), each single cell accommodated approximately 150–200 nanoparticles. The limit of detection for *P. aeruginosa* was ~10 CFU/mL, which is roughly three times lower than that of *S. aureus*. This was probably due to the larger size of *P. aeruginosa* relative to *S. aeruginosa*, resulting in the production

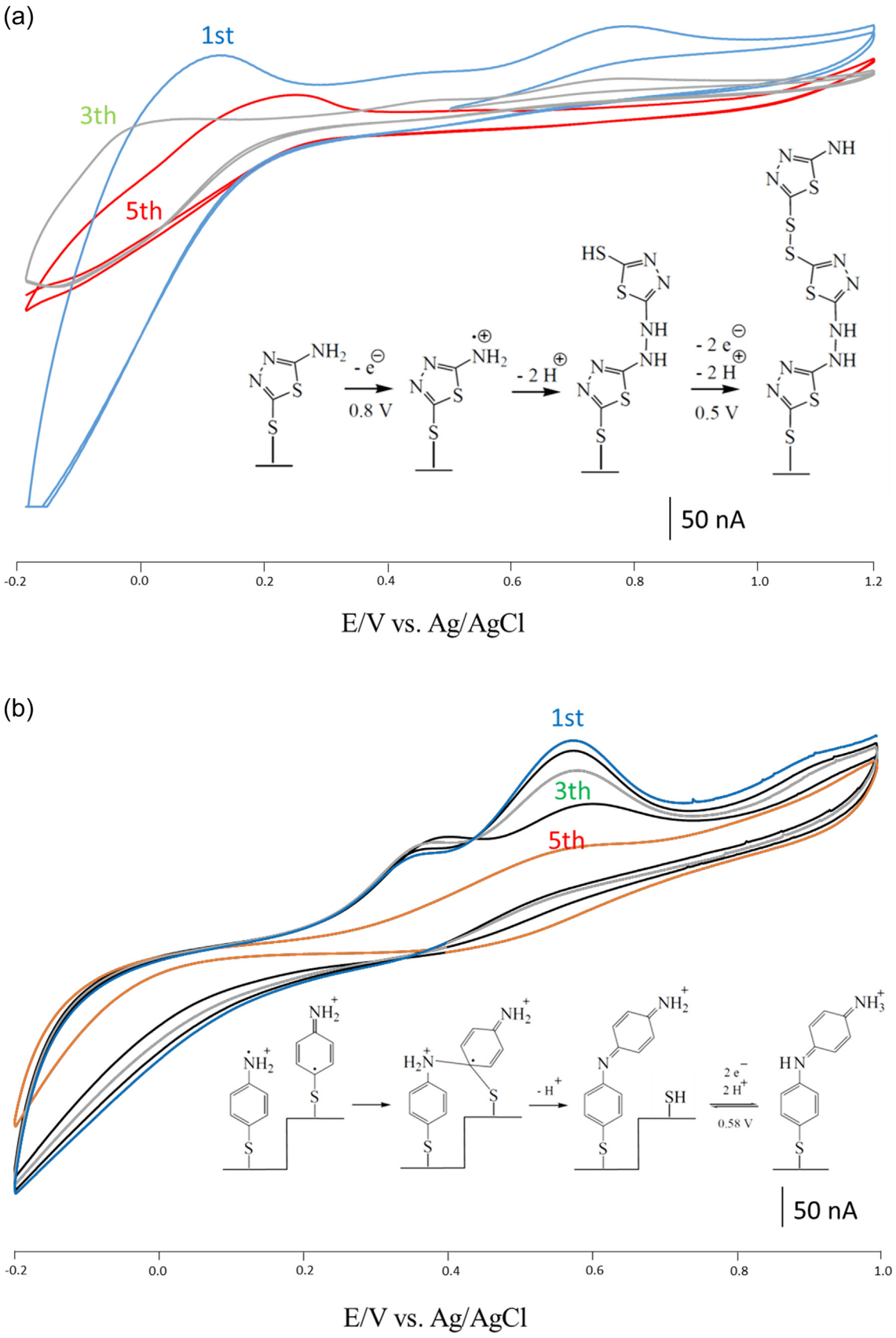

Fig. 5. Continuous Cyclic voltammograms (5 cycles) of GNPs modified with (a) 5-amino-2-mercapto-1,3,4-thiadiazole (AMT), and (b) 4-aminothiophenol (4-ATP) electropolymerization on surface of ITO electrodes.

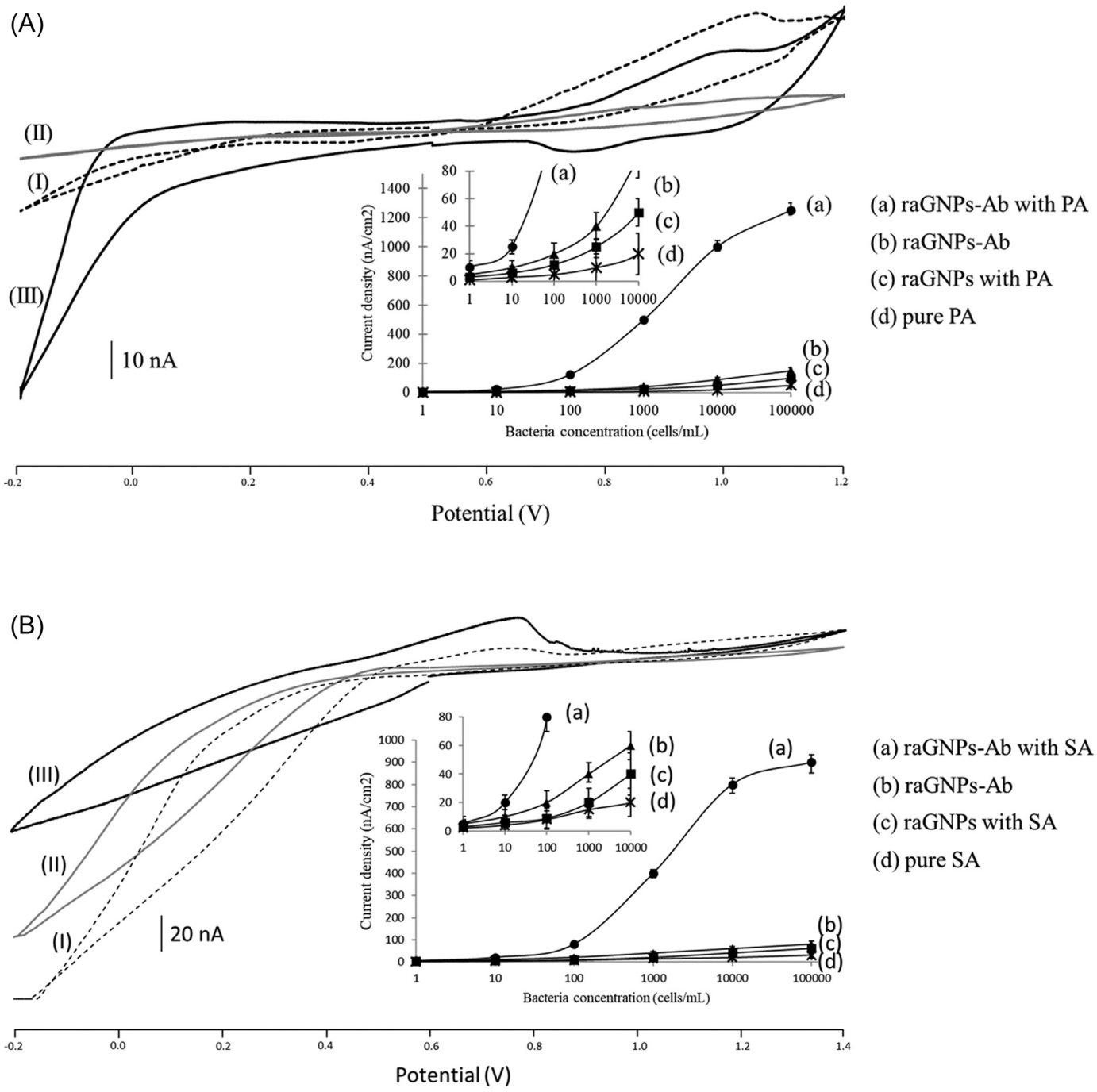

Fig. 6. Cyclic voltammograms (CV) showing the effect of the electropolymerized EAM layer on signal enhancement (bacteria concentration: (A) *P. aeruginosa* (PA), (B) *S. aureus* (SA) diluted to 10 CFU/mL using 100 mM HEPES + 20 mM phosphate buffer) under the following conditions: with (I) raGNPs-Ab (electropolymerized redox-active SAM + antibody conjugated GNPs; dash line); without (II) raGNPs-Ab (gray line), and (III) the control: raGNPs standard solution (solid line). All of the CVs were detected for a potential range from − 0.2 to + 1.2 V vs. counter/reference electrode. All measurements were obtained at a scanning rate of 100 mV/s. (total test volume, 100 μL).

of a significantly stronger electrochemical signal by increasing the number of modified GNPs conjugating on the surface of the bacteria. These results demonstrate the considerable potential of redox-active self-assembled monolayer GNPs as an electrochemical biosensor for the detection of several bacterial cells.

4. Conclusion

This paper reports the integration of advanced nanomaterial-based diagnostic technology, redox-active gold nano-particles (raGNPs), with a lab-on-chip microfluidic device, nano-sieving microfluidic system (NS-MFS), to produce a novel diagnostic system for *S. aureus* and *P. aeruginosa* in whole-blood. This study used raGNPs linked to bacteria to enhance the amperometric current via electropolymerization of electrochemically active molecules, such that the signals differ from those obtained using the traditional direct measurement of the redox reaction on the membrane of the bacteria. The proposed system has a detection limit of 10 CFU/mL and dynamic range of 10–10^5 CFU/mL for bacterial pathogens in human plasma. The system will have great potential to be applied in diagnosis of bacteremia.

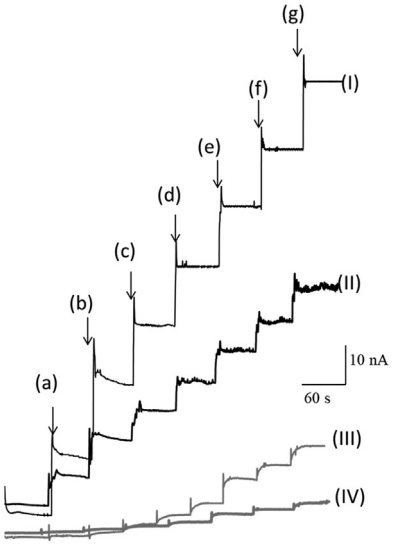

Fig. 7. Amperometric responses of p-AMT and p-ATP labelled GNPs for the successive detection of SA and PA in a 20 mM HEPES buffer: (I) E = 0.8 V, the p-AMT-GNPs in PA sample concentration (10–100 CFU/mL) added up to the volume of 10, 20, 30, 40, 50, 60, and 70 µL (a→g), (II) blood plasma samples spiked with p-AMT-PA under the same conditions in (I); (III) E = 1.0 V, pure p-ATP-SA sample concentration (10–100 CFU/mL) added up to the same conditions as those in panel I (a→g); (IV) blood plasma samples spiked with p-ATP-SA added up to the sample concentration in panel I (a→g).

Acknowledgments

We would like to thank the financial support from Ministry of Science and Technology, Taiwan from the project: 104-2221-E-007-072-MY3, 104-2321-B-007-003, 106-2622-E-007-020-CC2, 106-2923-E-007-004-MY3, 107-2622-E-007-006-CC2, 107-2221-E-007-012-MY3. This work was also financially supported by the Frontier Research Center on Fundamental and Applied Sciences of Matters, from The Featured Areas Research Center Program within the framework of the Higher Education Sprout Project by the Ministry of Education (MOE 107QR001I5), Taiwan.

Authors contribution

Chun-Wei Lee, data curation, analysis, validation and writing - original draft. Jen-Kuei Wu, conceptualization, methodology, supervision and writing - review. Hwan-You Chang, access to bio-samples and Writing - review. Fan-Gang Tseng, project administration, provide resources, supervision and writing - review & editing.

Appendix A. Supporting information

Supplementary data associated with this article can be found in the online version at doi:10.1016/j.bios.2019.03.040.

References

Afshari, A., Schrenzel, J., Ieven, M., Harbarth, S., 2012. Crit. Care 16.
Das, J., Aziz, M.A., Yang, H., 2006. J. Am. Chem. Soc. 128, 16022–16023.
Goggins, S., Marsh, B.J., Lubben, A.T., Frost, C.G., 2015. Chem. Sci. 6, 4978–4985.
Gzil, P., Vervoort, N., Baron, G.V., Desmet, G., 2003. Anal. Chem. 75, 6244–6250.
Hou, H.W., Bhagat, A.A.S., Lee, W.C., Huang, S., Han, J., Lim, C.T., 2011. Micromachines 2, 319–343.
Inzelt, G., 2008. Conducting Polymers. Springer Berlin Heidelberg, Berlin, Heidelberg.
Lazcka, O., Campo, F.J., Del, Muñoz, F.X., 2007. Biosens. Bioelectron. 22, 1205–1217.
Lee, H., Yoon, T.J., Weissleder, R., 2009. Angew. Chem. - Int. Ed. 48, 5657–5660.
Li, Y., Gu, Y., Zheng, B., Luo, L., Li, C., Yan, X., Zhang, T., Lu, N., Zhang, Z., 2017. Talanta 162, 80–89.
Lim, J.W., Ha, D., Lee, J., Lee, S.K., Kim, T., 2015. Front. Bioeng. Biotechnol. 3, 1–13.
Lukkari, J., Kleemola, K., Meretoja, M., Ollonqvist, T., 1998. Langmuir 14, 1705–1715.
Maalouf, R., Fournier-Wirth, C., Coste, J., Chebib, H., Saïkali, Y., Vittori, O., Errachid, A., Cloarec, J.-P., Martelet, C., Jaffrezic-Renault, N., 2007. Anal. Chem. 79, 4879–4886.
Murray, P.R., Masur, H., 2012. Crit. Care Med. 40, 3277–3282.
Phaneuf, C., Mangadu, B., Piccini, M., Singh, A., Koh, C.-Y., 2016. Biosensors 6, 49.
Revin, S.B., John, S.A., 2011. Electrochim. Acta 56, 8934–8940.
Sage, A.T., Besant, J.D., Lam, B., Sargent, E.H., Kelley, S.O., 2014. Acc. Chem. Res. 47, 2417–2425.
Saha, K., Agasti, S.S., Kim, C., Li, X., Rotello, V.M., 2012. Chem. Rev. 112, 2739–2779.
Sanvicens, N., Pastells, C., Pascual, N., Marco, M.P., 2009. TrAC - Trends Anal. Chem. 28, 1243–1252.
Sin, M.L., Mach, K.E., Wong, P.K., Liao, J.C., 2014. Expert Rev. Mol. Diagn. 14, 225–244.
Vainshtein, I., Lee, R., 2014. Bioanalysis 6, 1939–1951.
Vashist, S.K., 2012. Diagnostics 2, 23–33.
Vasudev, A., 2013. FIU Electron. Theses Diss. 956.
Wang, J., Chen, G., Jiang, H., Li, Z., Wang, X., 2013. Analyst 138, 4427.
Wang, W., Feng, M., Kong, D., Liu, L., Song, S., 2015. Food Agric. Immunol. 26, 738–745.
Wang, W., Liu, L., Song, S., Xu, L., Kuang, H., Zhu, J., Xu, C., 2016a. Sci. China Mater. 59, 665–674.
Wang, W., Liu, L., Song, S., Xu, L., Zhu, J., 2017. Food Agric. Immunol. 28, 274–287.
Wang, W., Liu, L., Xu, L., Kuang, H., Zhu, J., Xu, C., 2016b. Part. Part. Syst. Charact. 33, 388–395.
Xu, M., Wang, R., Li, Y., 2016. Analyst 141, 5441–5449.
Zhang, R.Y., Amlani, I., Baker, J., Tresek, J., Tsui, R.K., Fejes, P., 2003. Nano Lett. 3, 731–735.
Zhao, X., Hilliard, L.R., Mechery, S.J., Wang, Y., Bagwe, R.P., Jin, S., Tan, W., 2004. Proc. Natl. Acad. Sci. USA 101, 15027–15032.
Zhuang, J., Tang, D., Lai, W., Xu, M., Tang, D., 2015. Anal. Chem. 87, 9473–9480.